Cancer Cell International

RESEARCH

Open Access

Long-term zinc treatment alters the mechanical properties and metabolism of prostate cancer cells

Jiri Navratil[1], Monika Kratochvilova[2], Martina Raudenska[1,2], Jan Balvan[1], Tomas Vicar[1,2], Katerina Petrlakova[1], Kanako Suzuki[1], Lucie Jadrna[4], Jiri Bursa[4], Martin Kräter[5,6], Kyoohyun Kim[5], Michal Masarik[1,2,3] and Jaromir Gumulec[1*]

Abstract

The failure of intracellular zinc accumulation is a key process in prostate carcinogenesis. Although prostate cancer cells can accumulate zinc after long-term exposure, chronic zinc oversupply may accelerate prostate carcinogenesis or chemoresistance. Because cancer progression is associated with energetically demanding cytoskeletal rearrangements, we investigated the effect of long-term zinc presence on biophysical parameters, ATP production, and EMT characteristics of two prostate cancer cell lines (PC-3, 22Rv1). Prolonged exposure to zinc increased ATP production, spare respiratory capacity, and induced a response in PC-3 cells, characterized by remodeling of vimentin and a shift of cell dry mass density and caveolin-1 to the perinuclear region. This zinc-induced remodeling correlated with a greater tendency to maintain actin architecture despite inhibition of actin polymerization by cytochalasin. Zinc partially restored epithelial characteristics in PC-3 cells by decreasing vimentin expression and increasing E-cadherin. Nevertheless, the expression of E-cadherin remained lower than that observed in predominantly oxidative, low-invasive 22Rv1 cells. Following long-term zinc exposure, we observed an increase in cell stiffness associated with an increased refractive index in the perinuclear region and an increased mitochondrial content. The findings of the computational simulations indicate that the mechanical response cannot be attributed exclusively to alterations in cytoskeletal composition. This observation suggests the potential involvement of an additional, as yet unidentified, mechanical contributor. These findings indicate that long-term zinc exposure alters a group of cellular parameters towards an invasive phenotype, including an increase in mitochondrial number, ATP production, and cytochalasin resistance. Ultimately, these alterations are manifested in the biomechanical properties of the cells.

Keywords Mechanobiology, Zinc, Actin, Cytoskeleton, Mitochondria, Vimentin, Metabolism, Cancer

*Correspondence:
Jaromir Gumulec
j.gumulec@med.muni.cz
Full list of author information is available at the end of the article

Introduction

Non-tumor prostate epithelial cells have been observed to accumulate citrate and produce most of their ATP via glycolysis. The current hypothesis assumes this occurs due to the inhibition of aconitase by high intracellular zinc levels. The human prostate gland contains extremely high zinc levels, which significantly affect mitochondrial citrate metabolism and terminal oxidation. This inhibition of aconitase leads to a truncated Krebs cycle and a drop in oxidative phosphorylation (OXPHOS), which is accompanied by an increase in aerobic glycolysis [1]. During prostate carcinogenesis, citrate-producing secretory epithelial cells in the prostate stop accumulating zinc and undergo a metabolic shift to malignant citrate-oxidizing cells that produce ATP primarily through OXPHOS. Increased glycolysis, typical for non-tumor prostate epithelial cells, becomes again a characteristic of advanced castrate-resistant prostate cancer [2, 3]. The increase in glucose uptake and glycolysis seems to be a common feature of both normal and cancer cells when they experience a phenotypic change in the epithelial-mesenchymal spectrum [4]. Growing evidence links epithelial-mesenchymal transition (EMT) to the promotion of prostate cancer metastasis. The underlying mechanism of EMT is provided through the reorganization of the cytoskeleton, which, in turn, manifests in the changes in the mechanical properties of individual cancer cells and multicellular tissues [5]. Such changes in the mechanical properties at multiple levels (molecular, cellular, and tissue level) are key drivers of cancer progression [5]. In addition, these cellular parameters are in close correlation with increased stemness and drug resistance [6]. Our understanding of the interplay between EMT, mechanical determinants of cancer progression, and metabolic reprogramming of prostate cancer, however, remains incomplete.

To model these processes, we utilized prostate cancer cell lines, including the 22Rv1 cell line, which retains epithelial characteristics [7], and the PC-3 cell line derived from bone metastasis which shows a shift towards a mesenchymal phenotype with enhanced vimentin and Caveolin-1 (CAV1) expression [8, 9]. It is noteworthy that PC-3 cells exhibit increased sensitivity to zinc compared to 22Rv1 cells. However, extended zinc exposure leads to zinc and cisplatin resistance and metabolic alterations accompanied by enhanced SOX2 expression. Despite the re-establishment of intracellular zinc accumulation, prostate cancer cells do not completely revert to a non-malignant phenotype [10, 11].

In this study, we elucidate the correlation between cytoskeletal architecture changes and OXPHOS reprogramming, with resultant effects on cellular stiffness and subcellular cell dry mass redistribution. Furthermore, we describe the dual effects of long-term zinc exposure on EMT, with the potential for both induction and suppression [12, 13]. Additionally, by computational modeling and using actin- and vimentin-targeting drugs we describe the association of biophysical properties with cellular metabolism.

Methods

Chemical and biochemical reagents

The Ham's F12 medium, the RPMI-1640 medium, mycoplasma free FBS were purchased from VWR International, LCC (Randor, PE, USA). Phosphate buffered saline (PBS), zinc(II) sulfate, sodium sulfate, zinc chloride, trypsin, Ethylenediaminetetraacetic acid (EDTA) were purchased from Merck KGaA (Darmstadt, Germany). LIVE/DEAD™ Viability/Cytotoxicity Kit (L3224) was purchased from ThermoFischer Scientific.

Cell culture

The 22Rv1 human cell line derived from primary prostate cancer and the PC-3 cells derived from a bone metastasis of 4-grade prostatic adenocarcinoma were used in the study. 22Rv1 expresses an androgen receptor, is weakly testosterone-sensitive, and is PTEN positive [14]. The PC-3 is androgen-independent and unresponsive, negative for p53 and PTEN [14, 15]. PNT1A is a non-tumor epithelial prostate cell line.

22Rv1 and PNT1A cells were cultured in RPMI-1640 medium with 10% FBS. PC-3 cells were cultured in Ham's F12 medium with 7% FBS. Both media were supplemented with 100 U/ml penicillin and 0.1 mg/ml streptomycin. Cells were cultured at 37 °C with 5% CO_2 in a humidified incubator (Sanyo, Japan). 22Rv1 was purchased from DSMZ-German Collection of Microorganisms and Cell Cultures GmbH (Braunschweig, Germany), PC-3 and PNT1A were purchased from Merck KGaA.

Zinc (II) treatments of cell cultures

During long-term zinc treatment, cells were cultivated with the constant presence of zinc(II) ions. The concentrations of zinc(II) in the media were determined to be 8.4 ± 1.3 µmol/l for RPMI and 19.5 ± 6.6 µmol/l for Ham's medium. These concentrations were increased gradually using zinc(II) sulfate by small changes of 25 µM or 50 µM. Cells were cultured at each concentration no less than 1 week before harvesting and the viability was checked before adding more zinc. This process naturally selected zinc-resistant cells. The total time of cultivation of cell lines in zinc(II)-containing media exceeded 1 year. The final concentrations of added zinc(II) sulfate in media, further designated as "long-term zinc", were 50 µM for PC-3, 400 µM for the 22Rv1 cell line and 150 µM for PNT1A, resulting in final concentrations of 70 µmol/l

for PC-3 treated with Ham's medium and 408 µmol/l for 22Rv1 and 158 µmol/l for PNT1A cultured in RPMI. No vehicle was added to the control conditions as sulfate does not affect growth, viability, and cell stiffness (Fig. S1a-c). Intracellular zinc(II) content increased extensively and proportionally to added zinc sulfate in the long-term zinc-treated cell lines. For details see [10, 11]. Sulfate was used as a vehicle for zinc instead of chloride because it is the least toxic anorganic zinc compound [16]. The concentrations used in the experiment had no effect on viability or stiffness (Fig. S1).

Atomic force microscopy

For the analysis of cell stiffness, the bioAFM microscope JPK NanoWizard 3 (JPK BioAFM, Berlin, Germany) was placed on the inverted optical microscope Olympus IX-81 (Olympus, Tokyo, Japan) and equipped with a motorized stage with a Petri dish heater. Atomic force microscopy (AFM) measurements were conducted with spherical probes. A spherical cantilever was prepared by attaching a 5.73 µm melamine sphere (microParticles, Berlin, Germany) to a tipless cantilever (SD-qp-CONT-TL, NanoWorld, Switzerland). Before each experiment, the sensitivity and spring constant of cantilevers were determined by the contact-free method in Bruker-JPK software. A force-distance curve (FDC) was recorded at each point of the cantilever approach/retract movement. Typical FDC parameters were: 15 µm extend/retract length, a setpoint value of 1 nN, a sample rate of 5000 Hz, and a speed of 20 µm/s. The retraction length of 15 µm was sufficient to overcome any adhesion between the tip and the sample and ensure that the cantilever had been completely retracted from the sample surface. The system operated under closed-loop control, and a temperature of 37 °C was maintained during the whole experiment. The Young's modulus I was calculated by fitting the JKR model on the FDCs measured as force maps (64×64 points) of the region containing either a single cell or multiple cells. JPK data processing and AtomicJ software were used for the batch processing of measured data. Statistics were done on n = 31 22Rv1, n = 31 22Rv1-zinc, n = 40 PC-3 and n = 24 PC-3 zinc cells pooled from multiple independent experiments.

In silico model of atomic force microscopy

Finite Element (FE) Modelling was employed to assess the role of the observed cytoskeletal protein content change in the mechanical response. The model accounts for the nucleus, cytoplasm and membrane as well as cytoskeletal components represented by a continuous actin cortex and interconnected network of discrete pre-stressed actin bundles (ABs), curved microtubules (MTs) and wavy intermediate filaments (IFs). For further details on the FE model, see Supplementary Material 1 and [17].

The computational setup mimics the experimental conditions: a rigid sphere with a diameter of 5.73 µm was indented into the adherent cellular model to the depth of 0.9 µm (10% of the cell height). In contrast to a real cellular body, the inner structure of the computational model is symmetric (see Fig. 6) but has been verified to sufficiently capture the experimentally determined mechanical behavior under various loads (e.g. [17, 18]). This enabled us to select a set of indentation points (see Fig. 6b) where the modifications in the underlying structures could induce the most different responses. The resulting response was then considered as average between all these 5 points.

Real-time deformability cytometry

Real-time deformability cytometry (RT-DC) was performed according to Rosendahl et al. [19] and was performed similarly like in Peltanova et al. [20] using an AcCellerator (Zellmechanik, Dresden, Germany) at 37 °C. Briefly, 48 h after seeding, the cells were stained for 20 min with 60 nM MitoTracker Red, trypsinized and prior analysis kept de-adhered on a roller for 30 min. Consequently, cells were transferred to the CellCarrier measurement buffer (Zellmechanik). Measurement was performed in 30×30 µm (cross-section) microfluidic chips using RT-DC at a flow of 0.240 µl/s using ShapeIn 2.0.8 software (Zellmechanik). The Young's modulus was calculated from deformation and cell area using ShapeOut 2.17, after filtering with the following setting: cell area parallel to flow 80–1000 μm^2 (removal of cell debris/multicellular clusters), porosity 1.00–1.05 (removal of damaged cells). The MitoTracker fluorescence intensity was measured as a mean of peak heights (FL2 maximum) per cell. Statistics were done on n = 8 22Rv1, n = 4 22Rv1-zinc, n = 16 PC-3 and n = 10 PC-3 zinc measurements pooled from two to four independent experiments.

Real-time cell metabolic assay

The assay to measure oxygen consumption rate (OCR) and extracellular acidification (ECAR) was performed similarly like in Peltanova et al. [20]. Briefly, 10^4 cells per well were seeded in a Seahorse 8-well plate (Agilent Technologies, Santa Clara, CA, USA). The measurement was performed on the Seahorse XFp analyzer with Wave Controller 2.4 software (Agilent Technologies) using a Seahorse XF RPMI medium, pH 7.4 (Agilent). FCCP was used as an uncoupler of OXPHOS, and its concentration was optimized prior experiments for 500 nM for both 22Rv1 and PC-3. The experiment was repeated 2–3 times, each in biological triplicates to pentaplicates.

Flow-induced adhered cell deformation

The shear modulus of cells was determined using an approach based on Quantitative Phase Imaging (QPI) and shear flow-induced deformation of cells adhered in a microchannel, which we introduced previously [21]. Briefly, cells in Ibidi µ-Slide VI 0.1 (0.1 × 1.0 mm cross section) are exposed to 5 Pa shear stress pulses and based on the cell center of mass flow-induced shift a modulus was calculated using a Kelvin-Voigt model with a parametric deconvolution. For details see Vicar et al. [21]. The experiment was performed in triplicate to hexaplicate and repeated at least twice.

Protein extraction and proteome analysis

Extracted proteins were subjected to filter-aided sample preparation as described elsewhere [22]. Resulting peptides were analyzed by liquid chromatography–tandem mass spectrometry (LC–MS/MS) performed using UltiMate 3000 RSLCnano system (Thermo Fisher Scientific) online coupled with Orbitrap Q Exactive HF-X spectrometer (Thermo Fisher Scientific). LC–MS/MS data were processed using MaxQuant software. See Supplementary Material 1 for full details regarding the analyses and data evaluation.

MTT

The resistance to Cytochalasin D (CytD) was tested using an MTT assay. 22Rv1, PC-3 and zinc-resistant variants of the cells (10^4 cells per well) were seeded in the 96-well flat bottom plate and cultured under standard conditions for 48 h. To elucidate whether the vimentin is associated with or contributes to the development of resistance to actin polymerization inhibition by CytD, prior to the CytD treatment, one plate of PC-3 cells was pretreated with 10 nM vimentin depolymerizing Calyculin A (CalA) for 15 min. Then, the culture media was removed and replaced with fresh media with increasing concentration of CytD. After another 24 h, the solution containing CytD was replaced with fresh culture medium containing 5 mg/ml MTT and cells were incubated for 4 h. Finally, to dissolve formazan crystals, the medium was replaced with DMSO, and absorbance was determined at 570 nm (Cell plate reader Cytation 3, BioTek, VT, USA).

Cell growth analysis was performed on IncuCyte using 5-day label-free monitoring of cell growth. The cells were seeded to 96 well plate in 24plicates in a seeding density of 1000 cells/well. The cells were treated with 400 µM (for 22Rv1) and 50 µM (for PC-3) of $ZnCl_2$ and $ZnSO_4$. The concentration of Na_2SO_4 was calculated for the identical concentration of SO_4^{2-} as for $ZnSO_4$. Proliferation was measured for 5 days. After 5 days, cells were stained with a LIVE/DEAD™ Viability/Cytotoxicity Kit to measure the viability. The percentage of viable cells was defined as the ratio of red object count divided by red + green object count.

Wound healing assay

After passage, each cell line was resuspended and seeded into a 24-well plate. The optimal number of cells per well in 500 µl of medium was determined separately for each cell line: 300,000 cells for PC-3 and 350,000 cells for 22Rv1. After 24 h, the cells reached 100% confluency. The PC-3 CalA-pretreatment group was treated with CalA at a concentration of 10 nM for 15 min. Following this, a wound was created on the surface for all groups (PC-3 CalA-pre, control, long-term zinc, and control 22Rv1) using a yellow pipette tip. Cells were washed with PBS, then fresh medium (control) or medium with the test substance (60, 400 or 1200 nM CytD) was added. A photograph of each well was taken at time 0 and after 24 h at the same location. The images were analyzed using the TScratch program following the software instructions. The software calculated the percentage of the open wound area.

Refractive index tomography

Tomograms of refractive index (n) were captured using 3D Cell Explorer (Nanolive SA, Tolochenaz, Switzerland) with 60× magnification and using a custom-made optical diffraction tomography (ODT) setup with 63× magnification [23]. The cells were manually annotated for cell, nucleus, cytoplasm, and perinuclear region for which the average refractive index (n) was measured. Furthermore, a difference between n in the perinuclear area and cytoplasm (Δn) was calculated. From multimodal images of refractive index with MitoTracker staining using a custom-made ODT, the image correlation was calculated in the masks of cells.

Confocal microscopy

The distribution of Caveolin-1 (CAV1) and integrity of F-actin, β-tubulin, and vimentin after various treatments were studied using confocal microscopy. First, the cells were seeded on 18 mm coverslips coated with 20 µg/ml fibronectin and cultured under standard conditions for 48 h. Then, the cells were fixed in a pre-warmed fix solution containing 4% paraformaldehyde, 3% sucrose, PBS, and water for 20 min at 37 °C and washed three times with PBS. Right after, the cells were permeabilized using 0.2% Triton X-100 for 10 min. Permeabilization was followed by the blocking of non-specific Ab-blocking sites in PBS-BSA 0.1% for 60 min. Such prepared cells were incubated with primary antibodies (Vimentin, 1:200, V2258; Caveolin-1, 1:400, D46G3, Cell Signaling Technology, Danvers, Ma, USA; β-tubulin, 1:200, ab108342, Abcam; Cambridge, UK) according to the investigated

target for 90 min in 37 °C. Then, the cells were washed three times with PBS 0.05% Tween 20 (PBS-T) and incubated with compatible secondary antibodies (Alexa Fluor® 488, 1:750; Alexa Fluor® 647, 1:750) for 60 min in the dark at RT. F-actin was stained using Alexa Fluor™ 488 Phalloidin conjugate (Thermo Fisher Scientific, Waltham, Ma, USA) for 60 min in the dark at RT. After secondary antibody incubation, the cells were washed two times with PBS-T and then incubated with Hoechst. Prior to the mounting, cells were washed twice with PBS-T and once with PBS. Coverslips were mounted on glass slides using 7 µl of ProLong™ Gold Antifade Mountant (Thermo Fisher Scientific, Waltham, Ma, USA).

Confocal images were acquired with Laser scanning confocal microscope Zeiss LSM 880 with Airyscan-Fast module (Carl Zeiss, Cambridge, UK) using Plan-Apochromat 63×/1.40 objective, 405 nm and 633 nm solid-state lasers and 488 nm argon laser. DAPI was excited at 405 nm and emitted light was detected at 463 nm, Alexa Fluor® 488 was excited at 488 nm and detected at 562 nm, and finally, Alexa Fluor® 647 was excited at 633 nm and detected at 697 nm.

Statistical analysis

For statistics, t-test was used and in case of a problem of multiple comparisons, Benjamini-Hochberg-corrected p values were calculated. For the proteomic data, data were processed similarly like in Hanelova et al. [24]. Briefly, of 6482 identified proteins, 5074 had enough proteotypic peptides determined. LIMMA package in R was used for analysis. Over-representation analysis using the Gene Ontology database was performed using the clusterProfiler 4.0 package [25] and sample comparison was performed using compareCluster. For visualization, volcano plots [26], heatmaps (pheatmap package) [27] and, ggplot2 [28] were used. Furthermore, tidyverse and data.table [29] packages were used.

Results

Zinc-induced vimentin and EMT protein expression changes

Cell line models mimic different stages of cancer, as reflected by a different level of EMT. Compared to the 22Rv1 cell line derived from the primary tumor, the metastatic PC-3 cell line shows a shift towards a mesenchymal phenotype, as indicated by vimentin (VIM) and CAV1 expression. Vimentin and CAV1 were not detected in 22Rv1 cells. In addition to vimentin and CAV1, other proteins involved in EMT regulation were upregulated in PC-3 cells compared to 22Rv1 (see Fig. S2), such as COL1A1 [30], endoglin [31], integrin alpha-5/beta-1 (ITGA5:ITGB1), N-cadherin (CDH2), LAMB3, FNDC3B, and MMP14 [32, 33]. Furthermore, the expression of E-cadherin (CDH1) or CTNNA1 and 2 [34], which are associated with epithelial phenotype, was lower in PC-3 cells (Fig. S2a). However, other important markers of EMT, such as α-smooth muscle actin or FSP-1 were not expressed by PC-3 cells.

As a result of long-term zinc exposure (50 µM zinc sulfate), vimentin was fragmented in PC-3 cells

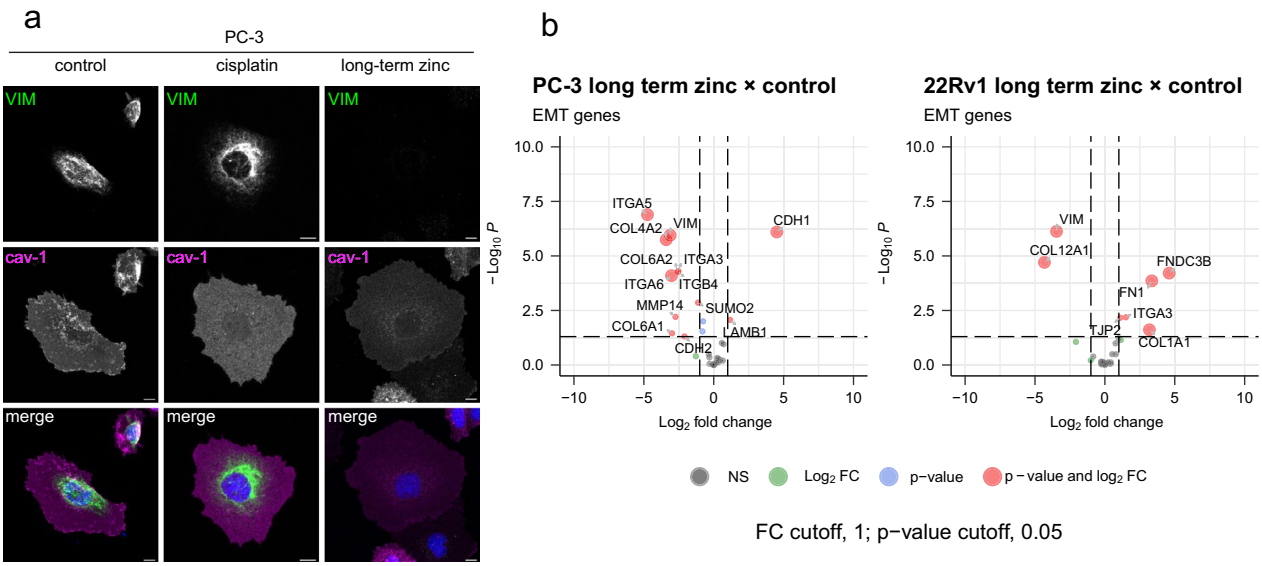

Fig. 1 Long-term zinc presence affects proteins associated with epithelial-mesenchymal transition. **a** Zinc-treated cells are characterized by a decrease in vimentin expression and an associated decrease in CAV1 membrane localization. Scale bar 10 µm **b** Volcano plots showing changes in EMT-associated proteins after long-term zinc exposure

(Fig. 1a, Table S2) and expressed in lower levels (Fig. 1b). In parallel with the decrease in vimentin, a redistribution of CAV1 from a predominantly membrane localization to the cytoplasm/perinuclear region was observed in long-term zinc-treated PC-3 cells (see Fig. 1a). It seems unlikely that this effect is caused by oxidative and cellular stress alone, as it does not occur after cisplatin treatment. (50 μM); see Fig. 1a.

Moreover, the expression of multiple other EMT-associated proteins was diminished in PC-3 cells following long-term zinc exposure (CDH2/N-cadherin, MMP14, ITGA5, SUMO2; as shown in Fig. 1b, Table S1). Nevertheless, the expression of CDH2 or MMP14 was still higher after zinc treatment in PC-3 compared to 22Rv1; see Fig. S2b. Long-term zinc exposure also increased the expression of E-cadherin (CDH1) in PC-3 cells, but this expression was still lower compared to 22RV1. Long-term zinc treatment induces an elevation in epithelial markers within PC-3 cells, representing a partial restoration towards the epithelial phenotype. However, zinc was not confirmed as a full consolidator of epithelial phenotype, as evidenced by the enhanced expression of specific EMT-associated proteins (COL1A1, FN1, FNDC3B) in 22Rv1 cells (Fig. 1b).

To demonstrate the generalizability of the results, the expression of EMT-associated proteins following long-term zinc exposure was tested on non-tumor prostate PNT1A cells. The results showed that, as observed in 22Rv1 cells, several integrin proteins (ITGB5 and ITGA2) were upregulated together with COL6A2 (Fig. S3a). In contrast, a reduction in ACTA2 and no change in VIM was observed in this cell line following zinc exposure. Apart from other than EMT-associated proteins, based on proteomic analysis the subset of commonly up- and down-regulated proteins by zinc seen in all three cell lines is biologically negligible (Table S3). This limited common effect of zinc suggests that the proteome changes are predominantly associated with cancer cells. Regarding other detected intermediate filaments, type I and II were not detected, type III exhibited no additional representants apart from VIM, type IV NES and NEFL demonstrated down-regulation in PC-3 cells exposed to zinc. In contrast, INA was up-regulated in both 22Rv1 and PC-3 cells exposed to zinc. Furthermore, Type IV LMNA, LMNB1 and B2 did not exhibit any alterations in expression following exposure to zinc (Table S1). In conclusion, our results suggests that long-term zinc exposure, while promoting an increase in epithelial characteristics, only partially reverts the cells to their original non-malignant epithelial state.

Long-term zinc impact on cellular refractive index and stiffness

In addition, the long-term presence of zinc induced changes in the cellular refractive index (RI), reflecting changes in cell mass density distribution. RI, which is calculated from phase shifts, corresponds to subtle changes in cell mass density distribution. It provides insight into detailed cell morphology and topography during various cellular processes, including cell death. In particular, cell dry mass can be calculated directly from the phase values detected in each pixel [35].

The long-term presence of zinc affected the total cellular RI. Interestingly, the RI was increased in 22Rv1 cells after zinc exposure (1.343 ± 0.004 vs. 1.347 ± 0.005), whereas it was decreased in PC-3 cells (1.3346 ± 0.05 vs. 1.340 ± 0.003, Fig. 2a, b). This decrease in RI in zinc-treated PC-3 cells could be attributed, at least in part, to a decrease in the abundance of proteins associated with the cell cortex (GO:0005938), cell surface (GO:0009986), nucleus (GO:0005634), or cytoplasm (GO:0005737) (Fig. 2c and Fig.S2c). Accordingly, expression of some cytoskeletal proteins such as actin (ACTB), members of the tubulin protein superfamily (TUBB8, TUBA1C, TUBB4A, TUBGCP4) or proteins involved in tubulin folding (tubulin-specific chaperone D) were also down-regulated (Table S2). Since actin filaments and tubulin microtubules are denser than the cytoplasm, their respective RI is also higher [36]. Previously discussed changes in vimentin, COL4A2 and COL6A1 (Fig. S2a, Fig. 1b), or MYO19 expression could also be involved in this phenomenon Table S2.

In addition to absolute changes in cellular RI in response to long-term zinc, a redistribution of mass density in the interior of the cells was observed. Specifically, an increase in perinuclear RI relative to the cell periphery was evident with long-term zinc, particularly in PC-3 cells (Fig. 2a, d).

The perinuclear region in which the RI increase was identified is typically characterised by a high amount of mitochondria. The data suggest this, as shown by the correlation between a RI (i.e., mass density) and mitochondrial staining (Fig. 2e, f). Interestingly, this correlation was more pronounced with long-term zinc exposure. (Fig. 2e). This correlation highlights the potential relationship between mitochondrial content and changes in mass density distribution and stiffness of the cells.

Notably, the change in cellular stiffness paralleled these changes in RI. Long-term zinc treatment resulted in a slight increase in cell stiffness for both cell lines. This increase was evident from Young's modulus determined using spherical cantilever in AFM and shear modulus measurements by flow stress induction of cell deformation (Fig. 3). The stiffness increase was

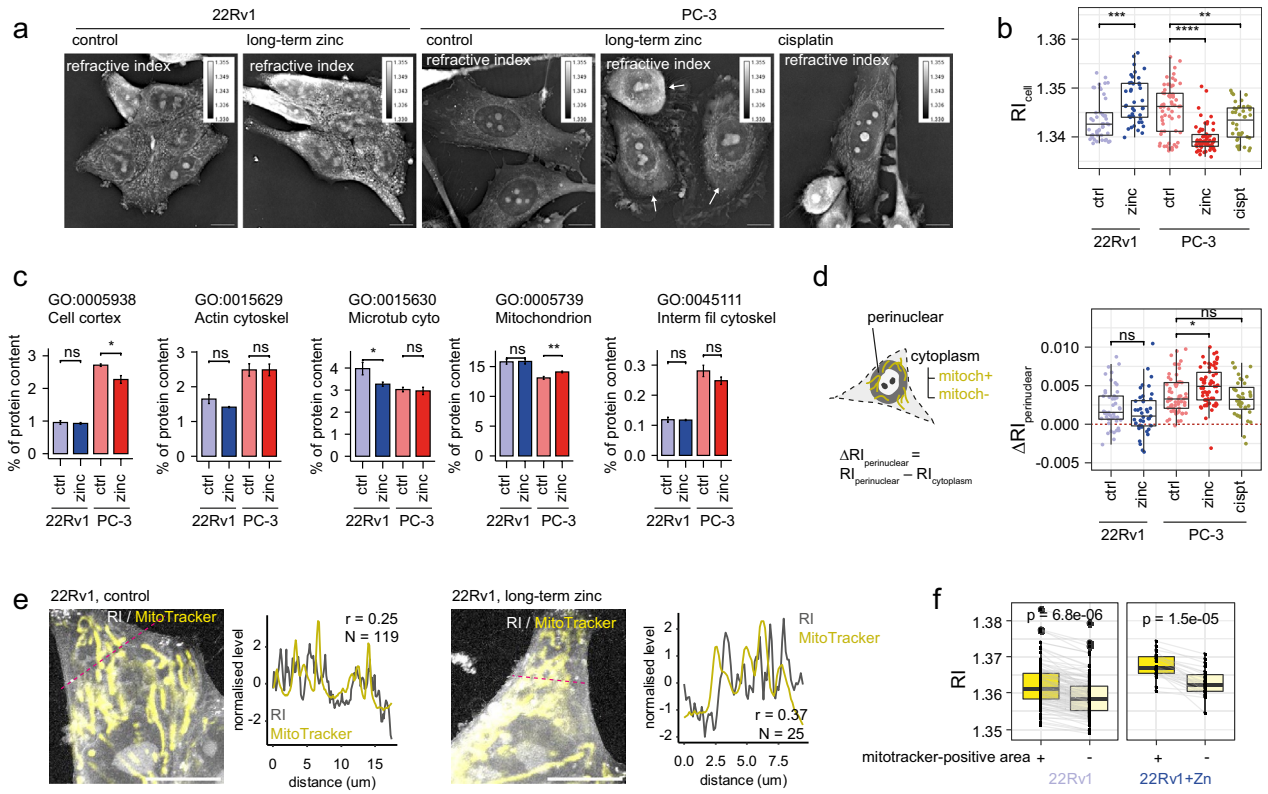

Fig. 2 Long-term exposure to zinc affects the cytoskeleton and thus the mechanical properties of cells. **a** Refractive index tomography. Zinc causes redistribution of phase-density in PC-3 cells towards the perinuclear region, this is not caused by oxidative stress (cisplatin). The scale bar indicates 10 µm. **b** Zinc treatment relatively increases RI perinuclearly in PC-3 cells. **c** Proportion of total cellular proteins proportional to the proteins of a given cytoskeletal cellular component (determined from riBAq). **d** The distribution of the refractive index corresponds subcellularly with the localization of mitochondria, the correlation is higher in cells affected by zinc. **e** MitoTracker + tomograms of the refractive index of long-term zinc-treated 22Rv1 cells and respective controls and profiles of both signals marked by a red dashed line. The correlation coefficient between the MitoTracker and RI signal is calculated from the pixel-based correlation averages of cells (N correspond to cell numbers). The scale bar indicates 10 µm. **f** Refractive indices in MitoTracker-positive and -negative areas. Lines connect MitoTracker positive and negative areas of identical cells (paired test)

long-term exposure-specific, as no significant stiffness increase was detectable in a short-term treatment (Fig. S1c). The relationship between mitochondrial content and cell stiffness was further confirmed using real-time deformability cytometry, where an increase in mitochondrial content positively correlated with cell stiffness (Fig. 3f, g). In addition, the observed long-term-zinc-associated increase on in cell stiffness was observed also in the non-tumor PNT1A cells (Fig S3b), indicating a relatively generalized effect of prostate cells.

In summary, long-term zinc exposure induces changes in cellular RI and stiffness. The interplay between the RI, influenced by mitochondrial content, and the redistributed mass density within the cells influences cellular mechanics, with implications for cancer aggressiveness.

Long-term zinc-drives changes in mitochondria and ATP production

To elucidate the potential link between increased mitochondrial content and alterations in cancer cell metabolism, we performed real-time cell metabolism assays. This technique allows the determination of ATP production mode and fundamental metabolic characteristics. Our results showed a significant increase in ATP production rate for both tumor and non-tumor cell lines following long-term zinc exposure (Fig. 4a, Fig S3c). Notably, both the glycolytic and mitochondrial ATP production pathways were enhanced.

Remarkably, the original metabolic preferences of each cell line were retained despite the increased ATP production. OXPHOS remained favored in 22Rv1 and PNT1A cells, whereas glycolysis prevailed in PC-3 cells. Using a glutamine-induced assay, we also demonstrated that,

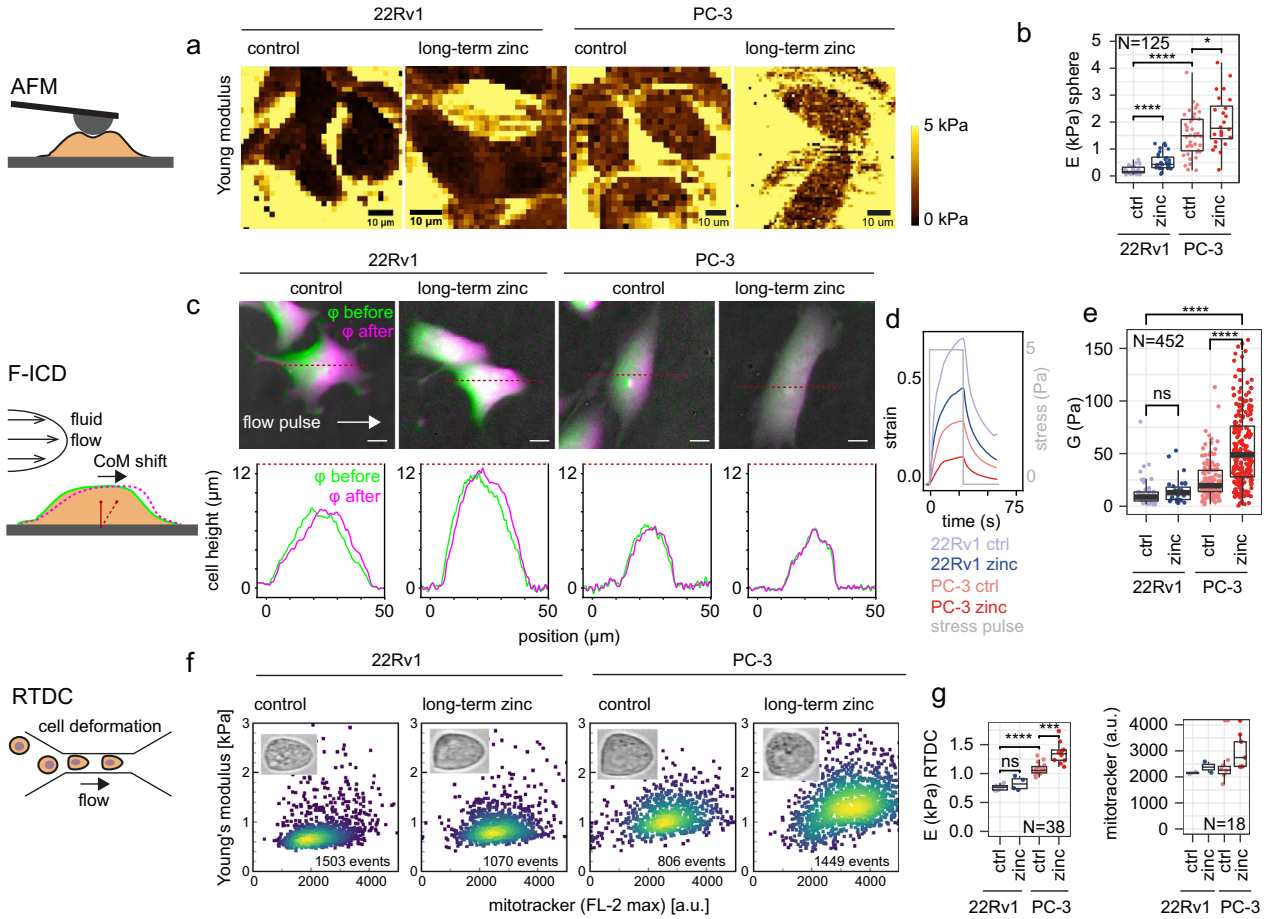

Fig. 3 Long-term exposure to zinc affects the cytoskeleton and thus the mechanical properties of cells. Young's modulus is higher in invasive PC-3 cells and increases with resistance, AFM spherical 5 um tip (**a**, **b**). **c** Flow-induced cell deformation (F-ICD); representative field of view. The scale bar indicates 10 µm, **d** Shear strain (centre of mass (CoM) shift divided by cell height) of cells after one 5 Pa shear stress pulse. **e** Shear modulus of cells calculated with the Kelvin-Voigt model, for details, see [21]. **f** Real-time deformability cytometry (RT-DC) of cells stained with MitoTracker (representative scatterplots), cells deformed in chamber shown in inset. **g** Young modulus and corresponding maximum MitoTracker fluorescence intensity for those cells determined from RT-DC

although glycolysis is a preferred pathway in PC-3, the ability to generate ATP by OXPHOS is preserved in these cells (Fig. S4).

Furthermore, long-term zinc exposure not only enhanced basal respiration but also increased the spare respiratory capacity of the tested cells (Fig. 4b). This observation implies an increased cellular oxygen demand under basal conditions and respiration closer to the theoretical maximum. The increase in spare respiratory capacity is particularly evident in 22Rv1 cells, where the spare capacity without the long-term zinc exposure is practically negligible. These predominantly oxidative cells also have a much higher coupling efficiency (Fig. 4b).

Biological process enrichment analysis revealed an increase in proteins involved in precursor metabolite and energy generation (GO:0006091), ATP metabolic process (GO:0046034), and epithelial cell proliferation (GO:0050673) in both cell lines (Supplementary Material 2). Since long-term exposure to zinc increases respiration, the question arises whether this is accompanied by a change in mitochondrial architecture—especially an increase in the network interconnectivity. Notably, we observed increased mitochondrial connectivity in PC-3 cells (Fig. 4d). However, no such changes were observed in 22Rv1 cells, suggesting that the effects of long-term zinc exposure on mitochondrial architecture may be cell-type-specific. Interestingly, these changes were not attributed to mitophagy, mitochondrial fusion, or fission (Fig. 4c), despite the concomitant increase in mitochondrial content in line with an increase in cell stiffness (Fig. 3c).

In addition, the expression of several cancer metabolism-related proteins was increased in both cell lines after long-term zinc exposure. These included

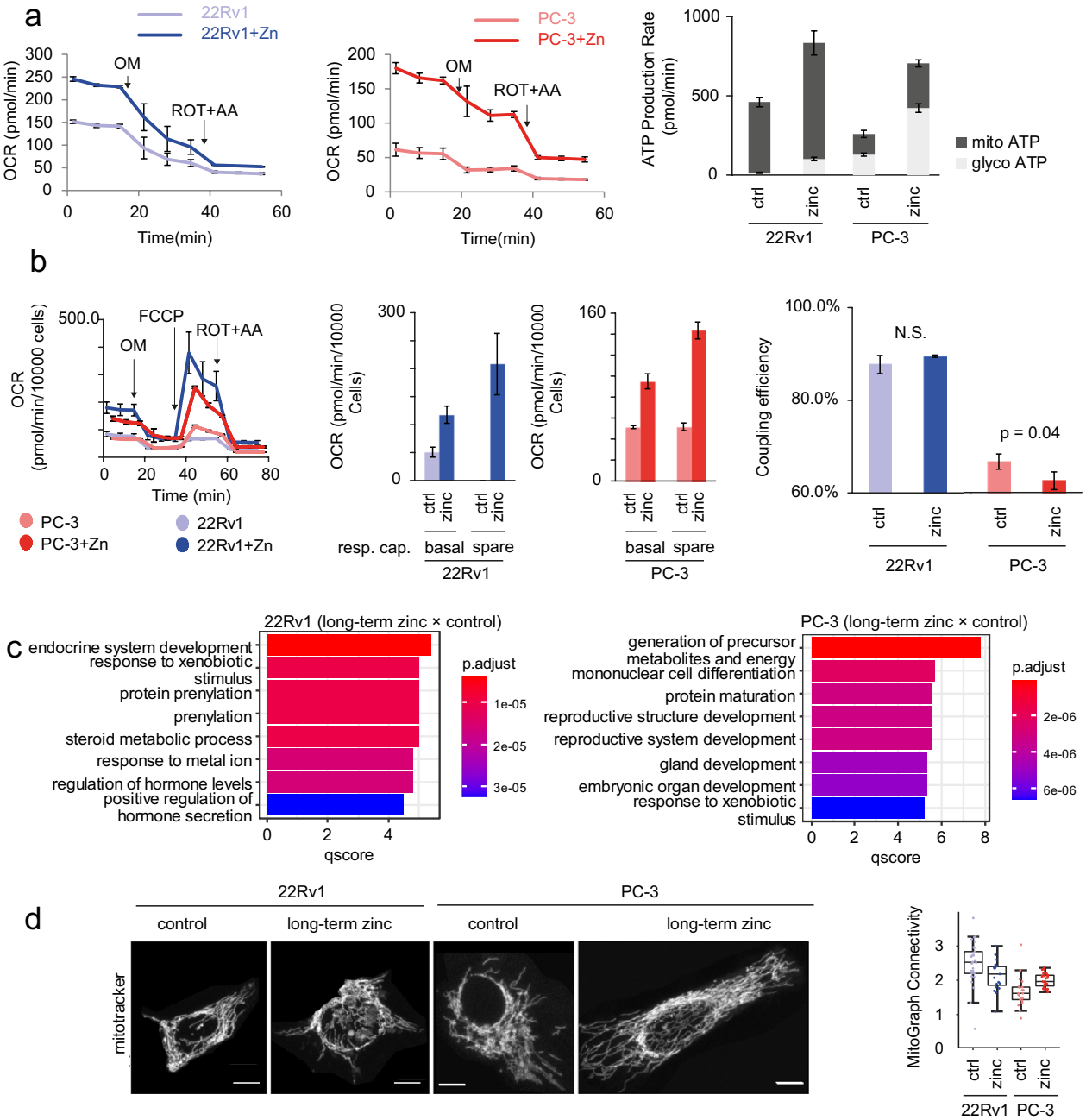

Fig. 4 Long-term zinc exposure affects mitochondrial ATP production and glycolysis. **a** Oxygen consumption rate (OCR) is increased in cells exposed to zinc indicating an increase in OXPHOS. ROT: rotenone; AA: antimycin A; OM: oligomycin. **b** Oxygen consumption rate (OCR) in cells exposed to 0.5 µM of uncoupler FCCP. Long-term zinc exposure increases spare respiratory capacity and, in PC-3, slightly decreases coupling deficiency. **c** Top 8 biological processes in long-term zinc treated (vs. control) cells. **d** Changes in spare respiratory capacity are not reflected in the mitochondrial architecture (MitoTracker staining, and Mitograph connectivity score). The scale bar indicates 10 µm

proteins such as argininosuccinate synthase (ASS1), transforming growth factor-β1 (TGF-β1) and β2 (TGF-β2), sodium/hydrogen exchanger 1 (NHE1), acid ceramidase (ASAH1), glutathione S-transferase kappa 1 (GSTK1), and Fatty acid desaturase 3 (FADS3). Conversely, the expression of glutamine synthetase (GS) and arginase II (ARG2) was downregulated (see Table S3).

Cytochalasin D resistance and linkage to vimentin fragmentation

To further elucidate the broad effects of long-term zinc exposure on cytoskeletal properties, we examined its effect on the sensitivity of PC-3 cancer cells to the actin polymerization inhibitor CytD. Interestingly, cells subjected to long-term zinc treatment exhibited altered responses to this drug. In untreated cells, 0.4 µM CytD (24 h treatment) inhibited actin polymerization, whereas long-term zinc-treated cells were resistant to such CytD concentration, and the inhibition of polymerization was partly absent even in concentrations up to 50 µM (Fig. 5a).

This relation prompted us to explore the potential link between the observed resistance to this actin-targeting drug and the mechanical properties of the cells, as previously studied in the context of the actin cytoskeleton and cell stiffness (section Long-term zinc Impact on Cellular Refractive Index and Stiffness). We hypothesized that the altered mechanical properties resulting from long-term zinc exposure might be a reason of the CytD resistance mechanism.

As previously mentioned, our observations revealed a distinct shift in vimentin expression and fragmentation in PC-3 cells compared to 22Rv1 cells, in response to long-term zinc exposure. This led us to investigate whether the

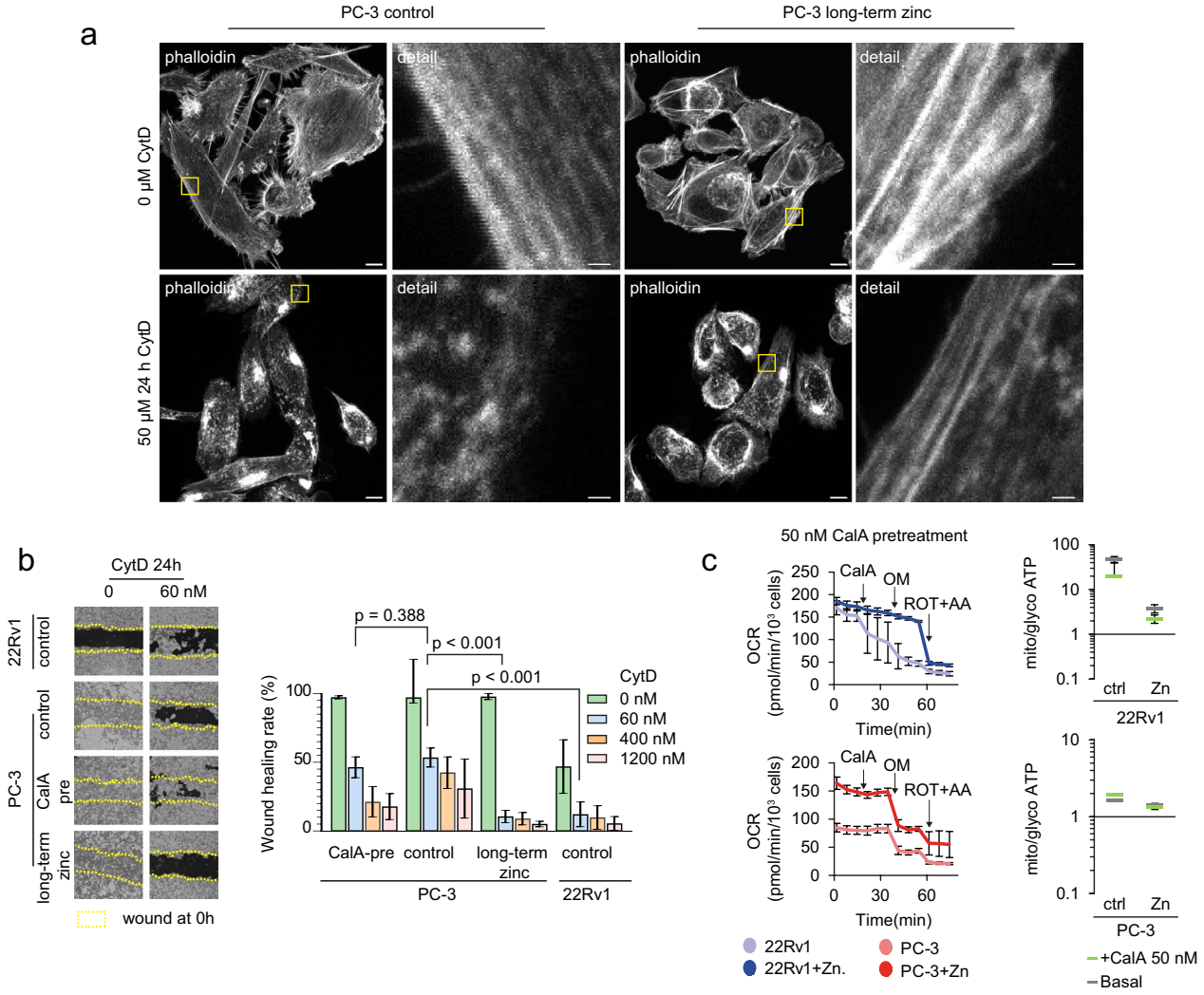

Fig. 5 Sensitivity of cells to actin polymerization inhibition by cytochalasin D (CytD). **a** Phalloidin staining of F-actin and CytD treatment of control and long-term zinc-treated PC-3 cells. Zinc caused the persistence of actin cables through the cells. The scale bar indicates 10 µm (1 µm in detail). **b** Wound healing assay of cells treated by CytD. Synergistic effect of vimentin phosphatase inhibitor Calyculin A (CalA) pre-treatment and long-term zinc exposure is shown. **c** 50 nM CalA effect on oxygen consumption rate (OCR) in an induced experiment. ROT: rotenone; AA: antimycin A; OM: oligomycin

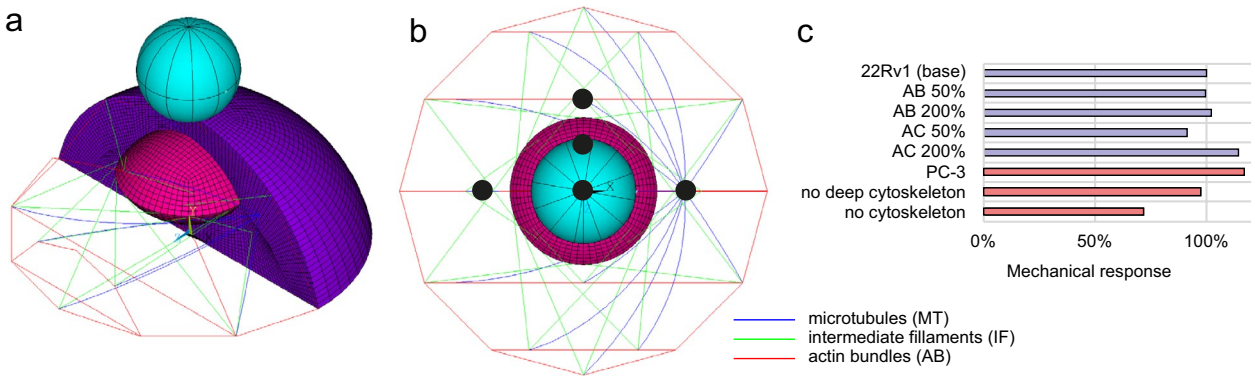

Fig. 6 In silico model of atomic force miscroscopy. Adherent cellular model shown with the indentor (cyan) at the apex (**a**). Top-view of the selected indentation points (black points) (**b**) in the context of cytoskeletal filaments (actin bundles (ABs), microtubules (MTs)s and intermediate filaments (IFs)) and nucleus in magenta-red. The cytoplasm in blue-magenta, actin cortex (AC) and membrane that encase cytoplasm not shown. Impact of the introduced modifications on the mechanical response (**c**), PC-3 cells are represented by double actin variant (in both AC and ABs)

vimentin is associated with or contributes to the development of resistance to actin polymerization inhibition by CytD. To explore this connection, we conducted an MTT assay to determine the sensitivity of various cell lines to CytD, including vimentin non-expressing 22Rv1 cells, zinc-untreated and zinc-treated PC-3 cells, and PC-3 cells pre-treated with a vimentin-depolymerizing agent, CalA [37].

Interestingly, zinc-treated PC-3 cells exhibited the highest resistance to CytD (IC50 = 23.2 μM), compared to the most sensitive 22Rv1 cells (IC50 = 4.2 μM). Surprisingly, pretreatment with CalA did not significantly alter resistance to CytD (24.6 μM for CalA-pretreated PC-3 vs 33.3 μM for zinc-adapted PC-3 cells). These results suggest that vimentin fragmentation (also associated with CAV1 redistribution, as shown previously in Fig. 1a) accompanies resistance but is not the primary cause.

Next, we determined whether the changes in cell stiffness induced by zinc-mediated alterations in the actin and vimentin cytoskeletons were reflected in cell migration. Wound-healing assays were performed and demonstrated that vimentin disruption modulated by CalA pretreatment did not contribute to a decrease in migration rate following actin disruption by CytD in PC-3 cells (Fig. 5b). However, contrary to CalA pretreatment, long-term zinc (which also causes VIM expression decrease), causes a significant decrease in migration rate after CytD treatment.

Furthermore, we investigated the metabolic consequences of CalA-induced vimentin disruption. Our results from CalA-induced metabolic assays revealed that predominantly glycolytic PC-3 cells exhibited insensitivity to CalA, regardless of long-term zinc exposure (Fig. 5c). Conversely, oxidative 22Rv1 cells exhibited a marked decrease in mitochondrial respiration, as indicated by the decrease in OCR. Importantly, since these cells do not express vimentin, the metabolism modulation is not directly related to vimentin disruption.

The collective findings indicate that while prolonged zinc exposure can protect actin from the inhibitory impact of CytD on actin polymerization, this protection is not invariably reflected in migration rates. Additionally, the effects of vimentin depolymerization appear to be coincidental rather than causal.

Proteins that may be involved in the emergence of higher chemoresistance in zinc-treated PC-3 cells include KCTD3 (log 9.8-fold change), IKBKB (log 5.8-fold change), CYP1B1 (log 5.3-fold change), AURKB (log 5.3-fold change), NOTCH2 (log 2.9-fold change), KIF4A (log 1.9-fold change), SOD2 (log 1.8-fold change), or PIKFYVE (log 5.6-fold change). For other proteins altered by zinc treatment of PC-3 cells, see Fig. S5 and Table S3-S4. According to molecular function enrichment analysis, the expression of proteins included in protein serine/threonine/tyrosine kinase activity (GO:0004712) was also enhanced by long-term zinc treatment in PC-3 cells (Supplementary Material 2).

Determinants of cell stiffness: biophysical insights

Finite element modeling was performed to show whether changes in cytoskeletal content determined by proteomic analysis alone could account for the increase in Young's modulus observed after long-term exposure of cells to zinc (Fig. 3a, b). Microtubule content did not differ between cells in response to zinc (Table S5), only actin and VIM did. To reflect the contribution of actin and vimentin, using an in silico model of AFM, we introduced modifications of both actin cortex (AC) and actin bundles

(ABs) content to 50% and 200%, reflecting the relative change of these components between zinc-exposed and unexposed PC-3 cells as well as PC-3 relative to 22Rv1 serving as base (more details in Supplementary Material 1, Table S5). Such an increase in AC resulted in an increase in Young's modulus to 117% in the model, compared to 133% increase (long-term zinc-treated PC-3 vs. control) or 690% increase (PC-3 vs. 22Rv1) determined by AFM (see Fig. 6, table S4). Similar changes in intermediate filament (IF) content showed an even smaller effect on cell stiffness in the deformation range studied, increasing only at large deformations.

To further understand the overall impact of the cytoskeleton as a whole on the AFM response in the computational setup, both the deep cytoskeleton (ABs, microtubules (MTs) and IFs) and the AC were removed; the resulting change in the mean stiffness was below 30% which is in agreement with our previous studies [17].

Because the modeled changes in Young's modulus are smaller than the measured ones, and because the organization of the actin network did not change, as seen in confocal imaging (Fig. 5a), there may be another, as yet-uncovered, mechanical contributor, such as other subcellular organelles or cytoskeletal crosslinkers not included in the model.

Discussion

Failure in intracellular zinc accumulation is a key process in prostate cancerogenesis. Although prostate cancer cells can accumulate zinc after long-term exposure, chronic zinc oversupply may accelerate prostate carcinogenesis or chemoresistance [10, 38]. Accordingly, in comparison with nonusers, men who consumed more than 100 mg/day of supplemental zinc had a higher relative risk of advanced prostate cancer [38].

A critical parameter which drives the progression of cancer is the change in mechanical properties at cellular and tissue level [5]. These properties are mostly driven by the reorganisation of individual cytoskeletal components, thereby enabling cell migration and invasiveness, all in relation to the biophysical properties of the surrounding microenvironment [39, 40]. The invasion of cells, changes in cell shape, and matrix remodelling require cells to expend energy [41]. While significant research has been performed to understand the cellular and molecular mechanisms guiding metastatic migration, less is known about cellular energy regulation [41] and in particular, how the biophysical parameters of cancer cells and, specifically for prostate cancer, how zinc dysregulation is involved in these processes.

An important marker of prostate cancerogenesis is a rise in ATP production caused by lower intracellular zinc levels [42]. Although long-term exposure to zinc leads to partial restoration of intracellular zinc accumulation [11], we found that ATP production is not decreased. On the contrary, long-term zinc treatment promoted both types of ATP production (glycolytic and mitochondrial) in 22Rv1 and PC-3 cells. Both cell lines retained a higher proportion of the originally preferred type of metabolism, OXPHOS was preferred in 22Rv1 and glycolysis in PC-3 cells. Long-term zinc exposure also enhanced the basal respiration and spare respiratory capacity [43, 44] of tested cells depicting their higher energetic efficiency. On the contrary, normal prostate epithelial cells have a very low reserve capacity [45]. As the cells with a lower spare respiratory capacity are more susceptible to oxidative stress [46], the enhancement of basal and spare respiratory capacity can reflect the higher energetic plasticity of zinc-treated cells and their higher resistance to oxidative stress. The higher resistance to oxidative stress in zinc-treated cells can also be caused by enhanced expression of GSTK1, ASAH1, or SOD2 in these cells [47–49]. Moreover, the expression of many proteins associated with cancer metabolism was enhanced in both cell lines after long-term zinc treatment (GO:0006091, GO:0046034, GO:0050673). Both lines had identically increased expression of ASS1, TGF-β1, TGF-β2, or NHE1. On the other hand, the expression of glutamine synthetase or arginase II was downregulated. Argininosuccinate synthetase 1 (ASS1) is the rate-limiting enzyme that catalyses arginine biosynthesis. Many malignant tumors are auxotrophic for arginine because ASS1 is silenced. Nevertheless, as we previously demonstrated, long-term zinc exposure enhances the ASS1 expression and the cellular pool of arginine [11]. Arginine was shown to induce metabolic gene expression involved in the OXPHOS pathway, glucose metabolism, fatty acid metabolism, and DNA metabolism [50]. Upregulation of ASS1 expression was also associated with resistance to glutamine starvation [51]. On the other hand, targeting purine synthesis enhanced the response to immune checkpoint inhibitors in ASS1-expressing tumors [52]. NHE1 can contribute to cell proliferation, cell motility, or invasion and can facilitate resistance to chemotherapy [53]. Increased NHE1 expression also comes along with an increased stiffness in melanoma cells. But in melanoma (MV3) cells it is rather the cortical stiffness that is affected [54]. TGFβ signaling stimulates arginine transport or synthesis of polyamines (prostate cancer cells maintain secretion of polyamines, but also are proliferative and therefore require high levels of intracellular polyamines [55]), is involved in stimulating both glycolysis and mitochondrial respiration and could be a major driver of EMT [56, 57].

Surprisingly, expression of some EMT-associated proteins was rather reduced in PC-3 cells (N-cadherin, MMP14, ITGA5, SUMO2) but enhanced in 22Rv1 cells

(COL1A1, FN1, FNDC3B) due to zinc treatment [32, 33, 58, 59]. Nevertheless, the expression of N-cadherin or MMP14 after zinc treatment was still higher in PC-3 compared to 22Rv1. Long-term zinc exposure also enhanced the expression of E-cadherin in PC-3 cells, but this expression was still lower compared to 22Rv1. Consequently, PC-3 cells still retain, at least partly, mesenchymal phenotype traits, compared to 22Rv1. Nevertheless, other important markers of EMT, such as α-smooth muscle actin (α-SMA), TWIST1 or FSP-1 were not expressed by PC-3 cells, both for long-term zinc-treated and untreated. This finding is inconsistent with Fontana et al., who detected α-SMA in PC-3 cells [60] and with Xue et al., who observed zinc in combination with paclitaxel to inhibit EMT by reducing TWIST1 expression in PC-3 cells [13] or with Zhang et al., who accordingly demonstrated EMT-promoting effect of zinc in ovarian cancer cells [61]. Short-term zinc treatments were, however used in these studies. Therefore, while long-term zinc treatment does bring PC-3 cells closer to an epithelial phenotype in certain aspects, it falls short of fully establishing this phenotype as observed in 22Rv1 cells.

Furthermore, long-term zinc presence led to changes in cellular RI, which reflects the cell mass density. While RI was enhanced in 22Rv1 cells after zinc exposure, it was decreased in PC-3 cells. Cells with stronger migration ability and weaker surface adherence were shown to manifest generally lower RI values [62]. The decrease in RI in zinc-treated PC-3 cells could also be partially explained by the drop in the abundance of cell cortex proteins, cell surface proteins, and proteins in the nucleus or cytoplasm. Actin (ACTB) was also downregulated. This suggests that ACTB is not a suitable housekeeping gene for monitoring protein expression in the presence of zinc. The expression of these proteins was not changed in 22Rv1 cells. However, considering the discussed metabolic changes conditioned by changes in mitochondrial activity in zinc-treated cells, it becomes clear that beyond absolute changes in RI, the redistribution of RI, i.e., mass density within the cells plays a crucial role. RI is closely correlated with mitochondria, which are protein- and lipid-rich structures. Consequently, mitochondria are the primary contributors to the elevated RI observed in the perinuclear region of cells as seen in QPI images.

In contrast to RI, the cell stiffness of both cell lines mildly increased in response to long-term zinc treatment. The results of computational simulations of AFM indicate that the impact of the change in cytoskeletal content determined by proteomic analysis, particularly actin and vimentin, on the mechanical response of cells in AFM is minimal between even 22Rv1 and PC-3 cells. Furthermore, the total change in cytoskeletal content between the long-term zinc-treated cells and the controls is even smaller (see Supplementary material 1, Table S5), suggesting that its impact on the mechanical response is estimated to be no more than a few percent, which is within the level of simulation inaccuracy. These results suggest there may be another yet-uncovered mechanical contributor such as other subcellular organelles, possibly mitochondria whose content was experimentally correlated with the cellular stiffness above. High mitochondria content was associated with prostate cancer disease progression [63]. The concurrent increase in mitochondrial content and cell stiffness suggests a potential interplay between cellular biophysics and energy metabolism.

Because vimentin is typically located perinuclearly and has been shown to enhance cell stiffness and provide resistance against compressive loads, adding another layer of complexity to the observed changes [64, 65], its role was investigated in long-term zinc-treated cells. Contrary to expectations, long-term zinc exposure led to a VIM decrease in VIM-expressing PC-3 cells and therefore, these intermediate filaments cannot be responsible for the increase in cell stiffness after long-term zinc exposure.

Furthermore, it is essential to consider the role of vimentin and its potential impact on cell stiffness measurements obtained by multiple techniques. The choice of measurement method may influence the extent to which vimentin contributes to cell stiffness. For instance, in AFM experiments, where primarily local deformation of the cell occurs and thus cortical actin is probed, the vimentin's role may be limited; the stiffness of IFs applies if their stretch exceeds 20% [66, 67] In contrast, techniques like Real-Time Deformation Cytometry (RT-DC) may capture global deformation of the cell with a broader range of cellular structures, potentially revealing vimentin's significance. This distinction is critical because vimentin fragmentation, as a result of zinc treatment, could have a more pronounced effect on global deformations, such as those observed in RT-DC experiments [66, 67].

The long-term zinc treatment also affected the sensitivity of PC-3 cancer cells to CytD. CytD binds the growing (+) end of actin microfilaments and stimulates ATP hydrolysis in formed G-actin dimers, thereby inhibiting polymerization and formation of viable microfilaments [68]. While actin filaments were disrupted due to 0.4 μM CytD in zinc-untreated cells, this effect did not occur in zinc-treated cells. This suggests that long-term zinc may stabilize actin, thereby reducing its dynamics to depolymerize. As pretreatment with CalA [37] did not significantly change resistance to CytD, and vimentin non-expressing 22Rv1 cells were the most sensitive to CytD, we can conclude that resistance to CytD is not

caused by fragmentation or depletion of vimentin, but that this phenomenon only accompanies the emergence of resistance in long-term zinc-treated PC-3 cells. Proteins that could be involved in the emergence of higher chemoresistance in zinc-treated PC-3 cells may be, for example, KCTD3 [69, 70], IKBKB [71], CYP1B1 [72], AURKB [73], NOTCH2 [74], KIF4A [75], SOD2 [76], or PIKFYVE [77]. High ATP production in zinc-treated cells may also contribute to cytochalasin resistance as the affinity of CytD decreases cooperatively with increasing ATP-G-actin concentration [78]. Taken together, these results suggest that long-term zinc exposure may offer a protective effect against the inhibitory influence of CytD on actin polymerization. However, intriguingly, this safeguarding of actin does not consistently manifest in migration rates.

Furthermore, vimentin depletion can cause CAV1 redistribution and may increase the CAV1 signaling activity due to the phosphorylation of CAV1 on Tyr14 [79, 80]. Activated CAV1 can promote chemoresistance by activating the WNT/β-Catenin pathway [81]. Activation of this pathway is also evidenced by increased expression of NOTCH2 or AURKB in zinc-treated PC-3 [82, 83]. The intriguing interplay between zinc exposure, actin dynamics, and cytochalasin resistance underscores the complexity of cancer cell responses to mechanical and biochemical cues. In this context, our findings align with the broader role of CAV1 as a potential orchestrator of cellular behavior in response to long-term zinc treatment. In essence, our study not only reveals the intricate interplay between zinc exposure, biophysical properties, and cellular adaptations but also opens doors to novel therapeutic avenues that consider the synergistic effects of mechanical and metabolic perturbations in the context of prostate cancer.

Conclusions

The alterations of mechanical properties of cells and tissues are associated with many diseases, including cancer. Part of the transitions between epithelial and mesenchymal phenotype, elastic and viscous properties of cells are driven by changes in cytoskeleton organization which facilitate cell invasion and therefore cancer progression [5]. Such changes are energetically demanding for cells, which, in turn, together with EMT/MET change mitochondrial processes, notably the OXPHOS.

In this study, we used a model of prostate cancer cells long-term-exposed to zinc to show a linkage between ATP production, mitochondrial distribution and biophysical parameters of prostate cancer cells. Long-term zinc treatment alters a spectrum of parameters associated with tumor cells and reduces the aggressiveness of those cells to a certain extent. However, the extent of this reduction is not sufficient. While long-term zinc treatment has been observed to return PC-3 cells to a more epithelial phenotype, characterized by decreased vimentin expression and enhanced E-cadherin expression, on the contrary, many of the cellular parameters are shifted towards a more aggressive phenotype. There is no evidence of a shift towards less efficient ATP production or sensitization of these cells to CytD. Long-term zinc-treated cells are more resistant and energetically efficient. Many signaling pathways related to chemoresistance are also activated in long-term zinc-treated cells. The cytochalasin resistance is accompanied by vimentin degradation and subcellular redistribution of cell dry mass and CAV1 to the perinuclear region.

Assuming the mechanisms described in this in vitro study are also valid at the tissue level, long-term zinc supplementation in prostate cancer patients would not be recommended, because zinc is not accumulated into cancer cells when administered in low concentrations and seems to support ATP production in cancer cells when administered in high concentrations. Our findings also suggest that zinc affects not only ATP production and epithelial-mesenchymal features but also cell migration, cell biomechanics, subcellular RI distribution, mitochondrial quantity and distribution, or cancer cell sensitivity to therapeutic drugs. Therefore, caution should be exercised in recommending zinc supplements to patients with prostate cancer and the exact effect of zinc on these important cellular parameters should be further investigated. In this study, we also proved that metabolic changes in cancer cells can be reflected in their stiffness and RI distribution. Therefore, using multiparametric analyses revealing links between cellular mechanics, energetics and tumor progression should be performed to provide a better understanding of prostate cancer pathogenesis.

Supplementary Information

The online version contains supplementary material available at https://doi.org/10.1186/s12935-024-03495-y.

Supplementary Material 1: Supplementary figures S1-S6, proteomic analysis and in silico model.

Supplementary Material 2. Proteomic analysis report.

Supplementary Material 3. Table S1: Proteome analysis of manually selected subset of EMT genes, 22Rv1 (long-term zinc-treated vs control) and PC-3 (long-term zinc-treated vs control), log2 fold changes (FC) and adjusted p value.

Supplementary Material 4. Table S2: Proteome analysis, unique 22Rv1 (long-term zinc-treated vs control) and PC-3 (long-term zinc-treated vs control) genes with 8-fold change log2 cutoff, up- and down-regulated genes shown separately. Enrichment analysis for biological process and cellular component enrichment calculated using string-db (version 11.5). 6482 proteins identified by proteome analysis used as background for correction.

Supplementary Material 5. Table S3: Proteome analysis, common long-term zinc-treated vs control, 1 log2 fold change threshold. Enrichment analysis for biological process and cellular component enrichment calculated using string-db (version 11.5). 6482 proteins identified by proteome analysis used as background for correction.

Supplementary Material 6. Table S4: AFM data for spherical tip (averages per cell), Young moduli calculated using JKR model.

Acknowledgements
This work was supported by the Ministry of Health of the Czech Republic NU22J-08-00062. We acknowledge the core facility CELLIM supported by MEYS CR (LM2018129 Czech-BioImaging). We thank the CEITEC MU Proteomics Core Facility of CIISB, Instruct-CZ Centre, supported by the Ministry of Education of the Czech Republic (LM2023042). Computational resources for proteomics data processing were provided by the e-INFRA CZ project (ID:90254), supported by the Ministry of Education, Youth and Sports of the Czech Republic. The short-term scientific mission of J. Gumulec was supported by the COST project Action COMULIS CA17121. A4L_ACTIONS, supported by European Union's Horizon 2020 under grant agreement No. 964997 and CIISB, Instruct-CZ Centre of Instruct-ERIC EU consortium, funded by MEYS CR infrastructure project LM2023042 and European Regional Development Fund-Project "UP CIISB" (No. CZ.02.1.01/0.0/0.0/18_046/0015974), is gratefully acknowledged for the financial support of the measurements at the CF Nanobiotechnology. This work has also received support from the Masaryk University Foundation (Grant No. MUNI/A/1587/2023). We appreciate help of Simon Vrana Klimovic from Nanobiotechnology Core Facility, CEITEC Brno for help with AFM analysis.

Author contributions
J.N. performed fluorescence microscopy, wrote manuscript. M.K. prepared long-term zinc-resistant cell variants, characterized them, performed metabolic analysis and wrote manuscript. M.R. conceptualized the research, wrote manuscript. J.B. performed quantitative phase imaging, T.V. performed image analysis and analyzed data, K.P. performed invasiveness, cytotoxicity and migration assays, K.S. analyzed mitochondria and cytoskeleton, L.J. and J.B. performed computational simulations and wrote manuscript. M.K. performed RTDC, K.K. performed ODT, M.M. managed the research team, wrote the manuscript. J.G. designed experiments, performed biophysical characterisation of cells, acquired funding, analyzed data, wrote manuscript.

Data availability
The mass spectrometry proteomics data have been deposited to the ProteomeXchange Consortium via the PRIDE partner repository with the dataset identifier PXD046410. Analyzed AFM data (Young moduli per cell) are available as supplementary material. Other data are available from the author upon request.

Declarations

Competing interests
MK is co-founder and shareholder of the Rivercyte GmbH, a company developing and selling deformability cytometry devices for blood cell analysis. AI-assisted technology ChatGPT was used in order check English grammar and linguistic clarity. After using this tool, the authors reviewed and edited the content as needed and takes full responsibility for the content of the publication.

Author details
[1]Department of Pathophysiology, Faculty of Medicine, Masaryk University, Kamenice 5, 625 00 Brno, Czech Republic. [2]Department of Physiology, Faculty of Medicine, Masaryk University, Kamenice 5, 625 00 Brno, Czech Republic. [3]BIOCEV, First Faculty of Medicine, Charles University, Prumyslova 595, 252 50 Vestec, Czech Republic. [4]Department of Biomechanics, Faculty of Mechanical Engineering, Brno University of Technology, Technicka 2, 61669 Brno, Czech Republic. [5]Max Planck Institute for the Science of Light, and Max-Planck-Zentrum für Physik Und Medizin, Staudtstraße 2, 91058 Erlangen, Germany. [6]Rivercyte GmbH, Henkestraße 91, 91052 Erlangen, Germany.

Received: 23 April 2024 Accepted: 30 August 2024
Published online: 11 September 2024

References

1. Costello LC, Franklin RB. A comprehensive review of the role of zinc in normal prostate function and metabolism; and its implications in prostate cancer. Arch Biochem Biophys. 2016;611:100–12.
2. Costello LC, Liu YY, Franklin RB, Kennedy MC. Zinc inhibition of mitochondrial aconitase and its importance in citrate metabolism of prostate epithelial cells. J Biol Chem. 1997;272:28875–81.
3. Ahmad F, Cherukuri MK, Choyke PL. Metabolic reprogramming in prostate cancer. Br J Cancer. 2021;125:1185–96.
4. Youssef KK, Nieto MA. Glucose metabolism takes center stage in epithelial-mesenchymal plasticity. Dev Cell. 2020;53:133–5.
5. Massey A, Stewart J, Smith C, Parvini C, McCormick M, Do K, et al. Mechanical properties of human tumour tissues and their implications for cancer development. Nat Rev Phys. 2024;6:1–14.
6. Montanari M, Rossetti S, Cavaliere C, D'Aniello C, Malzone MG, Vanacore D, et al. Epithelial-mesenchymal transition in prostate cancer: an overview. Oncotarget. 2017;8:35376–89.
7. Terry S, El-Sayed YI, Destouches D, Maillé P, Nicolaiew N, Ploussard G, et al. CRIPTO overexpression promotes mesenchymal differentiation in prostate carcinoma cells through parallel regulation of AKT and FGFR activities. Oncotarget. 2015. https://doi.org/10.18632/oncotarget.2740.
8. Bailey KM, Liu J. Caveolin-1 up-regulation during epithelial to mesenchymal transition is mediated by focal adhesion kinase. J Biol Chem. 2008;283:13714–24.
9. Kamibeppu T, Yamasaki K, Nakahara K, Nagai T, Terada N, Tsukino H, et al. Caveolin-1 and -2 regulate cell motility in castration-resistant prostate cancer. Res Rep Urol. 2018;10:135–44.
10. Holubova M, Axmanova M, Gumulec J, Raudenska M, Sztalmachova M, Babula P, et al. KRAS NF-kappa B is involved in the development of zinc resistance and reduced curability in prostate cancer. Metallomics. 2014;6:1240–53.
11. Kratochvilova M, Raudenska M, Heger Z, Richtera L, Cernei N, Adam V, et al. Amino acid profiling of zinc resistant prostate cancer cell lines: associations with cancer progression. Prostate. 2017;77:604–16.
12. Ninsontia C, Phiboonchaiyanan PP, Chanvorachote P. Zinc induces epithelial to mesenchymal transition in human lung cancer H460 cells via superoxide anion-dependent mechanism. Cancer Cell Int. 2016;16:48.
13. Xue YN, Yu BB, Liu YN, Guo R, Li JL, Zhang LC, et al. Zinc promotes prostate cancer cell chemosensitivity to paclitaxel by inhibiting epithelial-mesenchymal transition and inducing apoptosis. Prostate. 2019;79:647–56.
14. Fraser M, Zhao H, Luoto KR, Lundin C, Coackley C, Chan N, et al. PTEN deletion in prostate cancer cells does not associate with loss of RAD51 function: implications for radiotherapy and chemotherapy. Clin Cancer Res. 2012;18:1015–27.
15. Gumulec J, Balvan J, Sztalmachova M, Raudenska M, Dvorakova V, Knopfova L, et al. Cisplatin-resistant prostate cancer model: differences in antioxidant system, apoptosis and cell cycle. Int J Oncol. 2014;44:923–33.
16. Ni Shúilleabháin S, Mothersill C, Sheehan D, O'Brien NM, O'Halloran J, Van Pelt FNAM, et al. In vitro cytotoxicity testing of three zinc metal salts using established fish cell lines. Toxicol In Vitro. 2004;18:365–76.
17. Bansod YD, Matsumoto T, Nagayama K, Bursa J. A finite element bendotensegrity model of eukaryotic cell. J Biomech Eng. 2018. https://doi.org/10.1115/1.4040246.
18. Jakka VVSV, Bursa J. Finite element simulations of mechanical behaviour of endothelial cells. BioMed Res Int. 2021;2021: e8847372.
19. Rosendahl P, Plak K, Jacobi A, Kraeter M, Toepfner N, Otto O, et al. Real-time fluorescence and deformability cytometry. Nat Methods. 2018;15:355–8.
20. Peltanova B, Polanska HH, Raudenska M, Balvan J, Navratil J, Vicar T, et al. mRNA subtype of cancer-associated fibroblasts significantly affects key characteristics of head and neck cancer cells. Cancers. 2022;14:2286.
21. Vicar T, Chmelik J, Navratil J, Kolar R, Chmelikova L, Cmiel V, et al. Cancer cell viscoelasticity measurement by quantitative phase and flow stress induction. Biophys J. 2022;121:1632–42.

22. Wiśniewski JR, Ostasiewicz P, Mann M. High recovery FASP applied to the proteomic analysis of microdissected formalin fixed paraffin embedded cancer tissues retrieves known colon cancer markers. J Proteome Res. 2011;10:3040–9.
23. Kim K, Guck J. The relative densities of cytoplasm and nuclear compartments are robust against strong perturbation. Biophys J. 2020;119:1946–57.
24. Hanelova K, Raudenska M, Kratochvilova M, Navratil J, Vicar T, Bugajova M, et al. Autophagy modulators influence the content of important signalling molecules in PS-positive extracellular vesicles. Cell Commun Signal. 2023;21:120.
25. Wu T, Hu E, Xu S, Chen M, Guo P, Dai Z, et al. clusterProfiler 4.0: a universal enrichment tool for interpreting omics data. Innovation. 2021;2: 100141.
26. Blighe K, Rana S, Lewis M. EnhancedVolcano: publication-ready volcano plots with enhanced colouring and labeling. 2022.
27. Kolde R. pheatmap: Pretty Heatmaps. 2019.
28. Wickham H. ggplot2: elegant graphics for data analysis. New York: Springer-Verlag; 2016.
29. Dowle M, Srinivasan A. data.table: Extension of `data.frame`. 2023.
30. Wang Q, Shi L, Shi K, Yuan B, Cao G, Kong C, et al. CircCSPP1 functions as a ceRNA to promote colorectal carcinoma cell EMT and liver metastasis by upregulating COL1A1. Front Oncol. 2020;10:850.
31. Hu J, Guan W, Yan L, Ye Z, Wu L, Xu H. Cancer stem cell marker endoglin (CD105) induces epithelial mesenchymal transition (EMT) but not metastasis in clear cell renal cell carcinoma. Stem Cells Int. 2019;2019:9060152.
32. Kalluri R, Weinberg RA. The basics of epithelial-mesenchymal transition. J Clin Invest. 2009;119:1420–8.
33. Liu M, Qi Y, Zhao L, Chen D, Zhou Y, Zhou H, et al. Matrix metalloproteinase-14 induces epithelial-to-mesenchymal transition in synovial sarcoma. Hum Pathol. 2018;80:201–9.
34. Chi Q, Xu H, Song D, Wang Z, Ma G. α-E-Catenin (CTNNA1) inhibits cell proliferation, invasion and EMT of bladder cancer. Cancer Manag Res. 2020;12:12747–58.
35. Slabý T, Křížová A, Lošťák M, Čolláková J, Jůzová V, Veselý P, et al. Coherence-controlled holographic microscopy for live-cell quantitative phase imaging. In: Quantitative Phase Imaging. SPIE; 2015. p. 45–8.
36. Bon P, Lécart S, Fort E, Lévêque-Fort S. Fast label-free cytoskeletal network imaging in living mammalian cells. Biophys J. 2014;106:1588–95.
37. Eriksson JE, He T, Trejo-Skalli AV, Härmälä-Braskén AS, Hellman J, Chou YH, et al. Specific in vivo phosphorylation sites determine the assembly dynamics of vimentin intermediate filaments. J Cell Sci. 2004;117(Pt 6):919–32.
38. Leitzmann MF, Stampfer MJ, Wu K, Colditz GA, Willett WC, Giovannucci EL. Zinc supplement use and risk of prostate cancer. J Natl Cancer Inst. 2003;95:1004–7.
39. Moreno-Vicente R, Pavón DM, Martín-Padura I, Català-Montoro M, Díez-Sánchez A, Quílez-Álvarez A, et al. Caveolin-1 modulates mechanotransduction responses to substrate stiffness through actin-dependent control of YAP. Cell Rep. 2018;25:1622-1635.e6.
40. Levental KR, Yu H, Kass L, Lakins JN, Egeblad M, Erler JT, et al. Matrix crosslinking forces tumor progression by enhancing integrin signaling. Cell. 2009;139:891–906.
41. Zanotelli MR, Goldblatt ZE, Miller JP, Bordeleau F, Li J, VanderBurgh JA, et al. Regulation of ATP utilization during metastatic cell migration by collagen architecture. Mol Biol Cell. 2018;29:1–9.
42. Lin C, Salzillo TC, Bader DA, Wilkenfeld SR, Awad D, Pulliam TL, et al. Prostate cancer energetics and biosynthesis. Adv Exp Med Biol. 2019;1210:185–237.
43. Teh JT, Zhu WL, Newgard CB, Casey PJ, Wang M. Respiratory capacity and reserve predict cell sensitivity to mitochondria inhibitors: mechanism-based markers to identify metformin-responsive cancers. Mol Cancer Ther. 2019;18:693–705.
44. Nickens KP, Wikstrom JD, Shirihai OS, Patierno SR, Ceryak S. A bioenergetic profile of non-transformed fibroblasts uncovers a link between death-resistance and enhanced spare respiratory capacity. Mitochondrion. 2013;13:662–7.
45. Vayalil PK. Mitochondrial oncobioenergetics of prostate tumorigenesis. Oncol Lett. 2019;18:4367–76.
46. Sriskanthadevan S, Jeyaraju DV, Chung TE, Prabha S, Xu W, Skrtic M, et al. AML cells have low spare reserve capacity in their respiratory chain that renders them susceptible to oxidative metabolic stress. Blood. 2015;125:2120–30.
47. Sasagawa S, Nishimura Y, Okabe S, Murakami S, Ashikawa Y, Yuge M, et al. Downregulation of GSTK1 is a common mechanism underlying hypertrophic cardiomyopathy. Front Pharmacol. 2016;7:162.
48. Malvi P, Janostiak R, Nagarajan A, Zhang X, Wajapeyee N. N-acylsphingosine amidohydrolase 1 promotes melanoma growth and metastasis by suppressing peroxisome biogenesis-induced ROS production. Mol Metab. 2021;48: 101217.
49. Zaidi SK, Shen W-J, Cortez Y, Bittner S, Bittner A, Arshad S, et al. SOD2 deficiency-induced oxidative stress attenuates steroidogenesis in mouse ovarian granulosa cells. Mol Cell Endocrinol. 2021;519: 110888.
50. Chen C-L, Hsu S-C, Chung T-Y, Chu C-Y, Wang H-J, Hsiao P-W, et al. Arginine is an epigenetic regulator targeting TEAD4 to modulate OXPHOS in prostate cancer cells. Nat Commun. 2021;12:2398.
51. Long Y, Tsai WB, Wang D, Hawke DH, Savaraj N, Feun LG, et al. Argininosuccinate synthetase 1 (ASS1) is a common metabolic marker of chemosensitivity for targeted arginine- and glutamine-starvation therapy. Cancer Lett. 2017;388:54–63.
52. Keshet R, Lee JS, Adler L, Iraqi M, Ariav Y, Lim LQJ, et al. Targeting purine synthesis in ASS1-expressing tumors enhances the response to immune checkpoint inhibitors. Nat Cancer. 2020;1:894–908.
53. Stock C, Pedersen SF. Roles of pH and the Na(+)/H(+) exchanger NHE1 in cancer: from cell biology and animal models to an emerging translational perspective? Semin Cancer Biol. 2017;43:5–16.
54. Keurhorst D, Liashkovich I, Frontzek F, Nitzlaff S, Hofschröer V, Dreier R, et al. MMP3 activity rather than cortical stiffness determines NHE1-dependent invasiveness of melanoma cells. Cancer Cell Int. 2019;19:285.
55. Affronti HC, Rowsam AM, Pellerite AJ, Rosario SR, Long MD, Jacobi JJ, et al. Pharmacological polyamine catabolism upregulation with methionine salvage pathway inhibition as an effective prostate cancer therapy. Nat Commun. 2020;11:52.
56. Hua W, ten Dijke P, Kostidis S, Giera M, Hornsveld M. TGFβ-induced metabolic reprogramming during epithelial-to-mesenchymal transition in cancer. Cell Mol Life Sci. 2020;77:2103–23.
57. Durante W, Liao L, Reyna SV, Peyton KJ, Schafer AI. Transforming growth factor-β1 stimulates l-arginine transport and metabolism in vascular smooth muscle cells. Circulation. 2001;103:1121–7.
58. Bian T, Zheng L, Jiang D, Liu J, Zhang J, Feng J, et al. Overexpression of fibronectin type III domain containing 3B is correlated with epithelial-mesenchymal transition and predicts poor prognosis in lung adenocarcinoma. Exp Ther Med. 2019;17:3317–26.
59. Li B, Shen W, Peng H, Li Y, Chen F, Zheng L, et al. Fibronectin 1 promotes melanoma proliferation and metastasis by inhibiting apoptosis and regulating EMT. Onco Targets Ther. 2019;12:3207–21.
60. Fontana F, Raimondi M, Marzagalli M, Sommariva M, Limonta P, Gagliano N. Epithelial-to-mesenchymal transition markers and CD44 isoforms are differently expressed in 2D and 3D cell cultures of prostate cancer cells. Cells. 2019;8:143.
61. Zhang R, Zhao G, Shi H, Zhao X, Wang B, Dong P, et al. Zinc regulates primary ovarian tumor growth and metastasis through the epithelial to mesenchymal transition. Free Radic Biol Med. 2020;160:775–83.
62. Sun L, Wang Y, Zhang H, Min C, Zhang Y, Zhang C, et al. Graphene-based confocal refractive index microscopy for label-free differentiation of living epithelial and mesenchymal cells. ACS Sens. 2020;5:510–8.
63. Grupp K, Jedrzejewska K, Tsourlakis MC, Koop C, Wilczak W, Adam M, et al. High mitochondria content is associated with prostate cancer disease progression. Mol Cancer. 2013;12:145.
64. Jansen KA, Donato DM, Balcioglu HE, Schmidt T, Danen EH, Koenderink GH. A guide to mechanobiology: where biology and physics meet. Biochim Biophys Acta BBA-Mol Cell Res. 2015;1853:3043–52.
65. Mendez M, Restle D, Janmey P. Vimentin enhances cell elastic behavior and protects against compressive stress. Biophys J. 2014;107:314–23.
66. Janmey PA, Euteneuer U, Traub P, Schliwa M. Viscoelastic properties of vimentin compared with other filamentous biopolymer networks. J Cell Biol. 1991;113:155–60.
67. Wang N, Stamenović D. Contribution of intermediate filaments to cell stiffness, stiffening, and growth. Am J Physiol Cell Physiol. 2000;279:C188-194.

68. Trendowski M. Exploiting the cytoskeletal filaments of neoplastic cells to potentiate a novel therapeutic approach. Biochim Biophys Acta BBA - Rev Cancer. 2014;1846:599–616.
69. Angrisani A, Di Fiore A, De Smaele E, Moretti M. The emerging role of the KCTD proteins in cancer. Cell Commun Signal. 2021;19:56.
70. Freire-Benéitez V, Pomella N, Millner TO, Dumas AA, Niklison-Chirou MV, Maniati E, et al. Elucidation of the BMI1 interactome identifies novel regulatory roles in glioblastoma. NAR Cancer. 2021;3: zcab009.
71. Yang Z, Liao J, Cullen KJ, Dan H. Inhibition of IKKβ/NF-κB signaling pathway to improve Dasatinib efficacy in suppression of cisplatin-resistant head and neck squamous cell carcinoma. Cell Death Discov. 2020;6:36.
72. Zhu Z, Mu Y, Qi C, Wang J, Xi G, Guo J, et al. CYP1B1 enhances the resistance of epithelial ovarian cancer cells to paclitaxel in vivo and in vitro. Int J Mol Med. 2015;35:340–8.
73. Zhang Y, Jiang C, Li H, Lv F, Li X, Qian X, et al. Elevated Aurora B expression contributes to chemoresistance and poor prognosis in breast cancer. Int J Clin Exp Pathol. 2015;8:751–7.
74. Xiu MX, Liu YM. The role of oncogenic Notch2 signaling in cancer: a novel therapeutic target. Am J Cancer Res. 2019;9:837–54.
75. Pan LN, Zhang Y, Zhu CJ, Dong ZX. Kinesin KIF4A is associated with chemotherapeutic drug resistance by regulating intracellular trafficking of lung resistance-related protein. J Zhejiang Univ Sci B. 2017;18:1046–54.
76. Chien C-H, Chuang J-Y, Yang S-T, Yang W-B, Chen P-Y, Hsu T-I, et al. Enrichment of superoxide dismutase 2 in glioblastoma confers to acquisition of temozolomide resistance that is associated with tumor-initiating cell subsets. J Biomed Sci. 2019;26:77.
77. Chakraborty AR, Vassilev A, Jaiswal SK, O'Connell CE, Ahrens JF, Mallon BS, et al. Selective elimination of pluripotent stem cells by PIKfyve specific inhibitors. Stem Cell Rep. 2022;17:397–412.
78. Carlier MF, Criquet P, Pantaloni D, Korn ED. Interaction of cytochalasin D with actin filaments in the presence of ADP and ATP. J Biol Chem. 1986;261:2041–50.
79. Shi X, Fan C, Jiu Y. Unidirectional regulation of vimentin intermediate filaments to caveolin-1. Int J Mol Sci. 2020;21:7436.
80. Jiu Y. Vimentin intermediate filaments function as a physical barrier during intracellular trafficking of caveolin-1. Biochem Biophys Res Commun. 2018;507:161–7.
81. Wang X, Lu B, Dai C, Fu Y, Hao K, Zhao B, et al. Caveolin-1 promotes chemoresistance of gastric cancer cells to cisplatin by activating WNT/β-Catenin pathway. Front Oncol. 2020. https://doi.org/10.3389/fonc.2020.00046.
82. Wang Z, Yu Z, Wang GH, Zhou YM, Deng JP, Feng Y, et al. AURKB promotes the metastasis of gastric cancer, possibly by inducing EMT. Cancer Manag Res. 2020;12:6947–58.
83. Mangolini M, Götte F, Moore A, Ammon T, Oelsner M, Lutzny-Geier G, et al. Notch2 controls non-autonomous Wnt-signalling in chronic lymphocytic leukaemia. Nat Commun. 2018;9:3839.

Publisher's Note